Reaction products of Sm2Zr2O7 with calcium-magnesium- aluminum-silicate (CMAS) and their evolution

Yinghua Wang
Beijing Institute of Technology
Zhuang Ma
Beijing Institute of Technology
Ling Liu (richrad@bit.edu.cn)
Beijing Institute of Technology https://orcid.org/0000-0001-5926-7058
Yanbo Liu
Beijing Institute of Technology

Research Article

Keywords: Sm2Zr2O7 ceramic, CMAS, reaction product, erosion

Posted Date: March 10th, 2021

DOI: https://doi.org/10.21203/rs.3.rs-294209/v1

Version of Record: A version of this preprint was published at Journal of Advanced Ceramics on October 27th, 2021. See the published version at https://doi.org/10.1007/s40145-021-0514-x.

Abstract

During flight, many silicates (sand, dust, debris, fly ash, etc.) are ingested by an engine. They melt at high operating temperatures on the surface of Thermal barrier coatings (TBCs) to form calcium-magnesium-aluminum-silicate (CMAS) amorphous settling. CMAS erodes TBCs and causes many problems, such as composition segregation, degradation, cracking, and disbanding. As a new generation of TBC candidate materials, rare-earth zirconates ($Sm_2Zr_2O_7$) have good CMAS resistance properties. The reaction products of $Sm_2Zr_2O_7$ and CMAS and their subsequent changes were studied by the reaction of $Sm_2Zr_2O_7$ and excess CMAS at 1350°C. After 1 h of reaction, $Sm_2Zr_2O_7$ powders were not completely eroded. The reaction products were Sm-apatite and c-ZrO_2 solutions. After 4 h of reaction, all $Sm_2Zr_2O_7$ powders were completely eroded. After 24 h of reaction, Sm-apatite disappeared, and the c-ZrO_2 solution remained.

Introduction

TBCs are used to limit the heat transfer through coatings and protect vital engine components from hot corrosion. However, high operating temperatures result in the melting of any silicate (sand, dust, runway, debris, fly ash, volcanic ash, etc.) that may be ingested by an engine. These molten silicates, commonly referred to as CMAS (calcium-magnesium-aluminum-silicate), cause severe degradation of TBCs and premature delamination, exposing the metallic components to dangerous hot gases[1,2,3].

The most commonly used TBC composition is 7 wt.% yttria-stabilized zirconia (7YSZ). However, 7YSZ shows poor resistance to CMAS infiltration. Therefore, significant research has been performed on searching for new TBC materials with good CMAS resistance. As a new generation of thermal barrier coating candidate materials, rare-earth zirconates (such as $Sm_2Zr_2O_7$) not only have low thermal conductivity, appropriate thermal expansion coefficients and high thermal stability but also have better CMAS resistance properties than 7YSZ. The results studied by Krause show that rare earth zirconates can resist CMAS erosion in the early stage of the reaction[4,5,6].

Therefore, the reactions of rare-earth zirconates and CMAS have been studied extensively. Most of these studies are devoted to studying the reaction products of rare-earth zirconates and CMAS, such as the study of Hengbei Zhao[7]. The results studied by Julie M. Drexler showed that $Sm_2Zr_2O_7$ and CMAS react to form Sm-apatite[8]. However, little attention has been given to the element proportion and crystal structure of Sm-apatite. Furthermore, evidence from previous research showed that $Sm_2Zr_2O_7$ also deteriorated slowly by CMAS with increasing penetration time. This phenomenon may be related to subsequent changes in reaction products in excess CMAS. Therefore, the reaction products of CMAS and $Sm_2Zr_2O_7$ were accurately determined in this paper, and subsequent changes in the reaction products were also studied.

Experimental Procedures

Sm_2O_3 (99.9%, Forsman, Beijing, China) and $ZrOCl_2{\cdot}8H_2O$ (99.5%, Forsman, Beijing, China) were employed as raw materials to produce $Sm_2Zr_2O_7$ powders by chemical coprecipitation. Sm_2O_3 powders and $ZrOCl_2{\cdot}8H_2O$ were dissolved in nitric acid (mass fraction 65%~68%, Sinopharm Chemical Reagent Co, Shanghai, China) and deionized water, respectively. The obtained solution was mixed and stirred to generate a homogeneous solution, followed by cautious addition to ammonia water (mass fraction 25%~28%, Sinopharm Chemical Reagent Co, Shanghai, China) until a gel-like precipitate was obtained. The precipitate was filtered with distilled water repeatedly. After drying at 100℃ for 24 h and calcination at 1250℃ for 5 h for crystallization, the resultant powders were ground and sieved to remove the coarse agglomerates. Then, the required $Sm_2Zr_2O_7$ powders for this study were obtained.

CMAS with a composition of 38CaO-5MgO-8$AlO_{1.5}$-49SiO_2 in mole ratio was used in this study. CaO (≥99.7%, Aladdin, Shanghai, China), MgO (≥99.7%, Aladdin, Shanghai, China) , Al_2O_3 (≥99.7%, Aladdin, Shanghai, China) , SiO_2 (≥99.7%, Aladdin, Shanghai, China) were weighed in molar ratios and suspended in alcohol. The mixture was fully mixed by planetary ball milling with absolute alcohol for 72 h at a speed of 350 rpm. The suspension was dried, and the mixed powders were then calcined at 1550℃ for 4 h and quenched in water. By repeating the above steps once, CMAS glass for this study was obtained. The $Sm_2Zr_2O_7$ powders were uniformly placed on the top surface of the CMAS glass, and then the samples were heat-treated at 1350 °C for 1 h, 4 h and 24 h before quenching in air at room temperature.

The phase composition of $Sm_2Zr_2O_7$ powders after reaction with CMAS was characterized by X-ray diffraction (XRD, X`Pert PRO MPD, PANalytical) using CuKα radiation. Data were digitally recorded in a continuous scan in the range of angles (2θ) from 10◦ to 80◦ with a scanning rate of 4◦/min. The microstructure and composition of $Sm_2Zr_2O_7$ powders after reaction with CMAS were examined by scanning electron microscopy (SEM, Philips S-4800, Hitachi Ltd., Yokohama, Japan) equipped with an energy spectrum analyzer (EDS). The reaction product analysis and elemental mapping of $Sm_2Zr_2O_7$ powders with CMAS after reaction were performed using transmission electron microscopy (TEM, TECNAI $G^2$20, FEI, USA) with an energy dispersive spectrometer (EDS). The specimen used in TEM was prepared by a focused ion beam instrument (FIB, Crossbeam 540, Carl Zeiss, German).

Results And Discussion

Fig. 1 shows the XRD pattern of the powders after reacting with $Sm_2Zr_2O_7$ and CMAS. Compared with the standard peak PDF card, two kinds of peaks of reaction products can be found in Fig. 1. One is basically the same as the standard peak of $Ca_2Sm_8(SiO_4)_6O_2$ (PDF#29-0365). The peaks of $Ca_2Sm_8(SiO_4)_6O_2$ offset to high angles because the $Ca_2Sm_8(SiO_4)_6O_2$ from the reaction has lattice distortion. The other peak is basically the same as the standard peak of c-ZrO_2 (PDF#26-0341). Therefore, there are only $Ca_2Sm_8(SiO_4)_6O_2$ and c-ZrO_2 in the reaction products. No $Sm_2Zr_2O_7$ remains in the powders.

The images and the EDS patterns of $Sm_2Zr_2O_7$ powders eroded for 1 h at 1350℃ are shown in Fig. 2. As seen in Fig. 2(a), the powders after reacting from $Sm_2Zr_2O_7$ and CMAS have two morphological

characteristics. One is the partly eroded powder (P1), and the other is the completely eroded powder (P2). Fig. 2(b) is an enlarged view of the partly eroded powder. As seen in Fig. 2(b), the partly eroded powder includes the light center area (Z1) and the dark shell area (Z2). There is a dividing line between the light center area and the dark shell area. According to the EDS pattern, the dark shell area has Ca, Si, Zr, and Sm elements. The light center area has Zr and Sm but no Ca or Si elements. Ca and Si elements only exist in the dark shell area.

To determine the composition of the light center area, TEM was used to analyze the sample. The transmission electron microscope bright field image of the light center area is shown in Fig. 3(a). Fig. 3 (b) shows the electron diffraction pattern of area S1. As shown in Fig. 3 (b), the space group is Fm-3m. Combined with the elemental proportion of S1, it can be determined that S1 is $Sm_2Zr_2O_7$. Other areas in Fig. 3(a) are tested in the same way; they are all $Sm_2Zr_2O_7$. This suggests that the light center area with Ca and Si free area is not eroded by CMAS. This dividing line is the boundary of the reaction zone and unreactive zone. This proves that the reaction product protects the $Sm_2Zr_2O_7$ ceramic from CMAS erosion.

To study the effect of reaction products on erosion, the boundary areas of the reaction zone and unreactive zone are analyzed by TEM, and the results are shown in Fig. 4. Fig. 4 (a) is a transmission electron microscope bright field image of the reaction boundary areas close to $Sm_2Zr_2O_7$. As shown in Fig. 4 (a), there is an obvious boundary between two different micromorphologies. As shown in the dotted line in the figure. The energy spectrum of the S2 and S3 areas on both sides of the dotted line was analyzed. The results are shown in Table 1. No element of CMAS is found in area S2. Ca and Si elements of CMAS are found in area S3. S3 is SAED analyzed, and the results are shown in Fig. 4 (c). The space group is Fm-3m. However, the lattice constant and the included angle are different from the standard value. This suggests that Ca and Si enter the lattice of $Sm_2Zr_2O_7$ and cause lattice distortion. Therefore, S2 is $Sm_2Zr_2O_7$, and S3 is an erosion product. Fig. 4 (b) is a transmission electron microscope bright field image of the reaction boundary areas close to CMAS. As shown in Fig. 4 (b), there are some small grains with different sizes, which include some spherical crystal grains (S4) and some rod crystal grains (S5). The energy spectra of areas S4 and S5 are analyzed, and the results are shown in Table 1. S4 and S5 are SAED analyzed, and the results are shown in Fig. 4 (d) and Fig. 4 (e). The space group of S4 is $P6_3/m$, and the space group of S5 is Fm-3m. Combining the XRD results and elemental proportions of S4 and S5, it can be determined that the spherical crystal grain (S4) is $Ca_2Sm_8(SiO_4)_6O_2$ and the rod crystal grain (S5) is a c-ZrO_2 solution. The light color area of S6 is SAEDP analyzed, and the results are shown in Fig. 4 (f). The electron diffraction pattern of S6 is diffuse scattering, which infers that S6 is amorphous. The results of the energy spectrum of S6 are shown in Table 1. Ca, Si, Mg and Al elements of CMAS are found in area S6. Therefore, S6 is CMAS. Compared with the elemental proportions of $C_{38}M_5A_8S_{49}$ and S6, the contents of Ca in S6 decreased significantly. From 38 at.% to 5 at.%. The contents of Al and Si in S6 increased. S6 is surrounded by $Ca_2Sm_8(SiO_4)_6O_2$ and c-ZrO_2 solutions, which dissolve part of Ca from S6. This leads to the content of Ca in S6 decreasing significantly.

In addition, there are loose areas after the reaction in Fig. 2(b). To study why protection against CMAS fails, the loose areas after reaction are analyzed by TEM, and the results are shown in Fig. 5. Fig. 5(a) is a TEM bright field image of the loose area after the reaction. As shown in Fig. 5(a), unlike the reaction boundary areas, the grains in this area are relatively loose. There is a large amount of residual CMAS. The closer to the CMAS direction, the larger the grain size. Fig. 5(c) is a TEM high-power bright field image of the loose area after the reaction. The rod crystal grains (S7) are larger than those in Fig. 4. Areas S8 are spherical crystal grains, and S9 is CMAS. The results of the energy spectra of S4 and S5 are shown in Table 1. Zr, Sm and Ca are found in area S7. Sm Ca, Si and Zr elements are found in area S8. S7 and S8 are SAEDP analyzed, and the results are shown in Fig. 5 (b) and Fig. 5 (d). Combined with the elemental proportions of S7 and S8, it can be determined that S7 is a c-ZrO_2 solution (the space group is Fm-3m) and S8 is $Ca_2Sm_8(SiO_4)_6O_2$ (the space group is $P6_3/m$). S9 is residual CMAS. Compared with the elemental proportions of $C_{38}M_5A_8S_{49}$ and S6, the content of Ca in S9 decreased significantly. This is consistent with S6. In addition, the content of Si in S9 Decreased from 49 at.% to 40.67 at.%. This is because $Ca_2Sm_8(SiO_4)_6O_2$ grain growth requires more Si from CMAS.

The usual apatite crystal (space group is $P6_3/m$) formula is $A^I_4A^{II}_6(SiO_4)_6O_x$. A^I and A^{II} are alkali metal ions (A^{1+}), alkali earth metal ions (A^{2+}) or rare earth ions (A^{3+}). X is determined by the ionic valence of A. The coordination numbers of A^I and A^{II} are 9 and 7, respectively. In Sm-apatite, A^I tends to be occupied by Ca^{2+} with a larger ion radius. A^{II} tends to be occupied by Sm^{3+} with a smaller ion radius. Because the radii of Ca^{2+} (118 pm) and Sm^{3+} (113 pm) are similar, Sm^{3+} may account for up to half the seat of A^I. Therefore, it forms $A^I_2A^{II}_8(SiO_4)_6O_2$ Sm-apatite, and the formula is $(Ca_2Sm_2)Sm_6(SiO_4)_6O_2$. According to the energy spectrum, the content of Sm in apatite is high. There is a small amount of Zr in the Sm-apatite. This is because Zr^{4+} may account for the seat of A^I or A^{II}. The radius of Zr^{4+} (72 pm) is smaller than those of Ca^{2+} and Sm^{3+}. Therefore, Zr^{4+} tends to occupy A^{II}. Due to the introduction of Zr^{4+}, to achieve charge conservation, the low valence cation should increase, and the high valence cation should decrease in A^I. Therefore, Ca^{2+} in A^I increases and Sm^{3+} decreases in A^I. The change in the number of cations causes vacancies to appear in A^I. It can be inferred that the chemical formula of Sm-apatite is $(Ca_{1+x}Sm_{1-y}E_{y-x})(Sm_{1-x}Zr_x)_6\ (SiO_4)_6O_2$, where E is the vacancy. In the following, it is called Sm-apatite for short.

The image of $Sm_2Zr_2O_7$ powders eroded for 4 h at 1350℃ is shown in Fig. 6(a). As shown in Fig. 6(a), all $Sm_2Zr_2O_7$ powders are eroded by CMAS. There are no partly eroded powders with core-shell structures. Fig. 6(b) shows only rod crystal grains (Z5) and spherical crystal grains (Z6). The elements of Z5 and Z6 are shown in Table 2. According to the reaction results for 1 h, rod crystal grains (Z5) are c-ZrO_2 solution, and spherical crystal grains (Z6) are Sm-apatite. This suggests that all $Sm_2Zr_2O_7$ powders are completely eroded by CMAS after a 4 h reaction. In addition, compared with the results of reaction for 1 h, it can be found that the contents of Sm, Ca and Si in c-ZrO_2 solution decrease.

The image of $Sm_2Zr_2O_7$ powders eroded for 24 h at 1350℃ is shown in Fig. 6(c). It can be found that there are only rod crystal grains in CMAS. No spherical crystal grains exist in this situation. The elements

of the spherical crystal grain (Z7 in Fig. 6(d)) are also shown in Table 2. Based on the previous results, the rod crystal grains are still c-ZrO_2 solutions. Compared with the results of the contents of elements in Z6, there is no Si in the c-ZrO_2 solution. The contents of Sm and Ca are reduced.

CMAS and $Sm_2Zr_2O_7$ react to form Sm-apatite and c-ZrO_2 solutions, which can block the diffusion of elements in CMAS at the beginning of the reaction. With increasing reaction time from 1 h to 4 h, the $Sm_2Zr_2O_7$ powders are completely eroded by CMAS. This is because of the excess CMAS in the reaction. Excessive CMAS makes the barrier fail. Compared with 1 h, the grains of the Sm-apatite and c-ZrO_2 solutions grew. However, from 4 h to 24 h, Sm-apatite gradually disappeared until it was gone completely. It is speculated that Sm-apatite is completely dissolved in excessive CMAS. The c-ZrO_2 solution remains.

According to the above process, the erosion model of excessive CMAS to $Sm_2Zr_2O_7$ material is established and shown in Fig. 7. First, CMAS melts at approximately 1200℃. Liquid CMAS spreads on the surface of $Sm_2Zr_2O_7$. Then, Ca and Si in CMAS mainly diffuse into $Sm_2Zr_2O_{7,}$ which results in lattice distortion of $Sm_2Zr_2O_7$. Zr and Sm in $Sm_2Zr_2O_7$ also diffuse into CMAS at the same time. When the content of Zr in CMAS is greater than its solubility, Zr will reprecipitate from CMAS to form c-ZrO_2. A small amount of Sm and Ca dissolve in c-ZrO_2. A c-ZrO_2 solution is formed. Meanwhile, Sm, which diffuses from $Sm_2Zr_2O_{7,}$ reacts with Ca and Si to form Sm-apatite. Because c-ZrO_2 solution grains are close to Sm-apatite grains, these grains constitute a dense barrier layer that can block the diffusion of the elements in CMAS. During the reaction, some small grains are devoured by large grains following Ostwald's rule. The c-ZrO_2 solution and Sm-apatite grains will grow. However, as the reaction time further increased, Sm-apatite gradually dissolved in CMAS. This may be because the solubility of Sm is higher than Zr in CMAS. Sm in Sm-apatite can diffuse into CMAS completely. However, Zr in c-ZrO_2 solution cannot. Therefore, only the c-ZrO_2 solution remains. The disappearance of Sm-apatite breaks the tight bond between the c-ZrO_2 solution and Sm-apatite. Therefore, the barrier layer will fail. CMAS will follow the above process and continue to erode $Sm_2Zr_2O_7$. It can be inferred that $Sm_2Zr_2O_7$ will be completely eroded if the reaction is long enough time. In the end, only some c-ZrO_2 solution grains remain.

Conclusion

The $Sm_2Zr_2O_7$ powders were uniformly placed on the top surface of the CMAS glass and heat-treated at 1350 °C for 1 h, 4 h and 24 h. After 1 h of reaction, $Sm_2Zr_2O_7$ powders were not completely eroded. Completely eroded powders and partly eroded powders with core-shell structures were formed. The reaction products were Sm-apatite and c-ZrO_2 solutions. Furthermore, because c-ZrO_2 solution grains were close to Sm-apatite grains, these grains constituted a dense barrier layer that can block the diffusion of the elements in CMAS. After 4 h of reaction, partly eroded powders disappeared, and all $Sm_2Zr_2O_7$ was eroded. The content of Sm-apatite in the reaction product decreased. The grains of Sm-apatite and c-ZrO_2 solution grew. After 24 h of reaction, Sm-apatite disappeared, and the c-ZrO_2 solution remained. The

disappearance of Sm-apatite broke the tight bond between the c-ZrO_2 solution and Sm-apatite, which is the main reason for barrier layer failure.

References

[1] Bravo Luis G.,Jain Nishan,Khare Prashant,Murugan Muthuvel,Ghoshal Anindya,Flatau Alison. Physical aspects of CMAS particle dynamics and deposition in turboshaft engines[J]. Journal of Materials Research,2020,35(17).

[2] S. Bakkar,M.V. Pantawane,J.J. Gu,A. Ghoshal,M. Walock,M. Murugan,M.L. Young,N. Dahotre,D. Berman,S.M. Aouadi. Laser surface modification of porous yttria stabilized zirconia against CMAS degradation[J]. Ceramics International,2020,46(5).

[3] Zhenwei Cai,Jishen Jiang,Weizhe Wang,Yingzheng Liu,Zhaomin Cao. CMAS penetration-induced cracking behavior in the ceramic top coat of APS TBCs[J]. Ceramics International,2019,45(11).

[4] Y.X. Kang,Y. Bai,G.Q. Du,F.L. Yu,C.G. Bao,Y.T. Wang,F. Ding. High temperature wettability between CMAS and YSZ coating with tailored surface microstructures[J]. Materials Letters,2018.

[5] Honglong Wang,Zhizhi Sheng,Emily Tarwater,Xingxing Zhang,Jeff W. Fergus. Function of Reaction Layer in Pyrochlore Thermal Barrier Coatings against CMAS Corrosion[J]. ECS Transactions,2015,66(18).

[6] G. Witz,V. Shklover,W. Steurer,S. Bachegowda,H.-P. Bossmann. High-temperature interaction of yttria stabilized zirconia coatings with CaO–MgO–Al 2 O 3 –SiO 2 (CMAS) deposits[J]. Surface & Coatings Technology,2015,265.

[7] Hengbei Zhao,Carlos G. Levi,Haydn N.G. Wadley. Molten silicate interactions with thermal barrier coatings[J]. Surface & Coatings Technology,2014,251.

[8] Julie M. Drexler,Angel L. Ortiz,Nitin P. Padture. Composition effects of thermal barrier coating ceramics on their interaction with molten Ca–Mg–Al–silicate (CMAS) glass[J]. Acta Materialia,2012,60(15).

Tables

Table 1						
at.%	Ca	Si	Sm	Zr	Mg	Al
S1	-	-	51.21	48.79	-	-
S2	-	-	50.75	49.25	-	-
S3	5.17	7.66	47.69	39.48	-	-
S4	15.32	40.06	42.82	1.80	-	-
S5	5.77	-	22.86	71.37	-	-
S6	13.50	60.16	-	-	6.27	20.07
S7	5.77	-	20.92	73.31	-	-
S8	16.28	40.78	40.26	2.66	-	-
S9	28.75	40.67	3.36	-	7.34	19.88

Table 2						
at.%	Ca	Si	Sm	Zr	Mg	Al
Z1	-	-	51.11	48.89	-	-
Z2	15.88	25.41	20.91	36.01	-	1.79
Z3	23.38	40.11	15.27	11.29	2.67	7.27
Z4	12.61	11.43	9.41	62.10	1.81	2.64
Z5	22.72	46.20	12.35	10.88	1.98	5.87
Z6	8.77	3.53	7.63	80.06	-	-
Z7	6.16	-	4.78	89.06	-	-

Figures

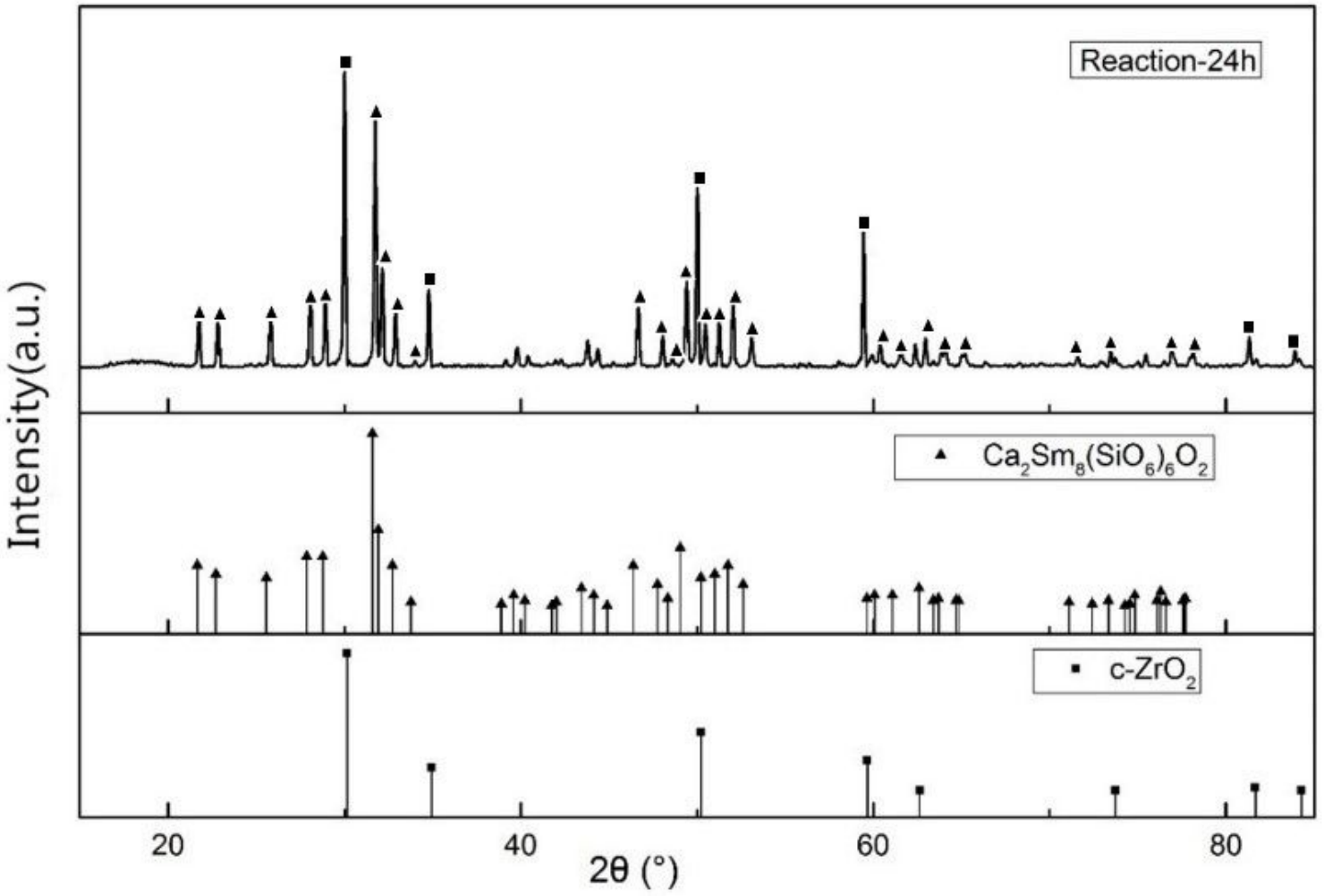

Figure 1

Compared with the standard peak PDF card, two kinds of peaks of reaction products can be found in Fig. 1.

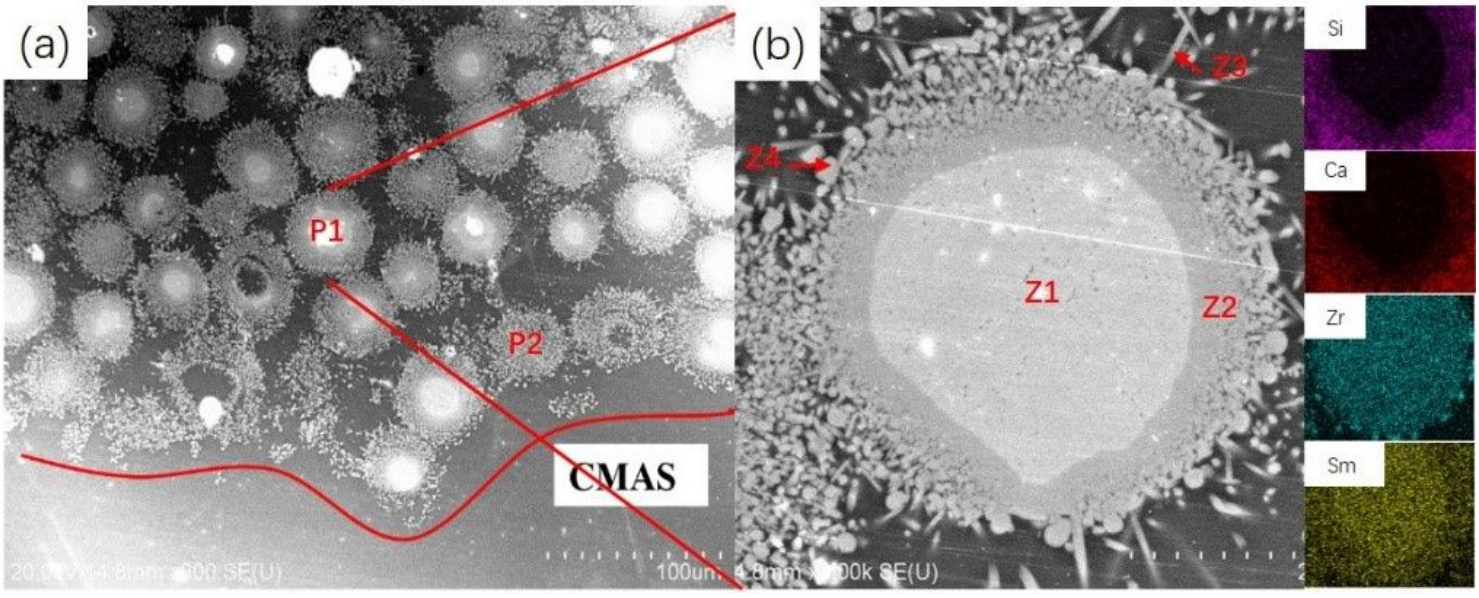

Figure 2

The images and the EDS patterns of Sm2Zr2O7 powders eroded for 1 h at 1350℃ are shown in Fig. 2. As seen in Fig. 2(a), the powders after reacting from Sm2Zr2O7 and CMAS have two morphological characteristics. One is the partly eroded powder (P1), and the other is the completely eroded powder (P2). Fig. 2(b) is an enlarged view of the partly eroded powder. As seen in Fig. 2(b), the partly eroded powder includes the light center area (Z1) and the dark shell area (Z2).

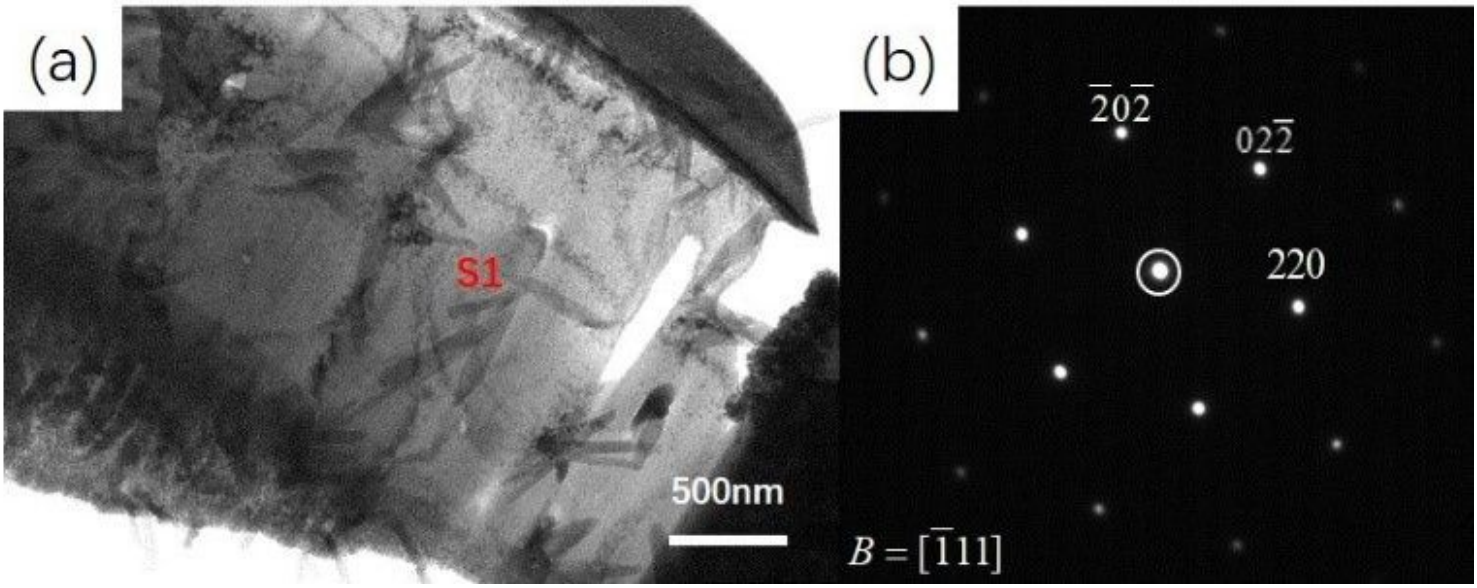

Figure 3

The transmission electron microscope bright field image of the light center area is shown in Fig. 3(a). Fig. 3 (b) shows the electron diffraction pattern of area S1. As shown in Fig. 3 (b), the space group is Fm-3m. Combined with the elemental proportion of S1, it can be determined that S1 is Sm2Zr2O7. Other areas in Fig. 3(a) are tested in the same way; they are all Sm2Zr2O7. This suggests that the light center area with Ca and Si free area is not eroded by CMAS. This dividing line is the boundary of the reaction zone and unreactive zone.

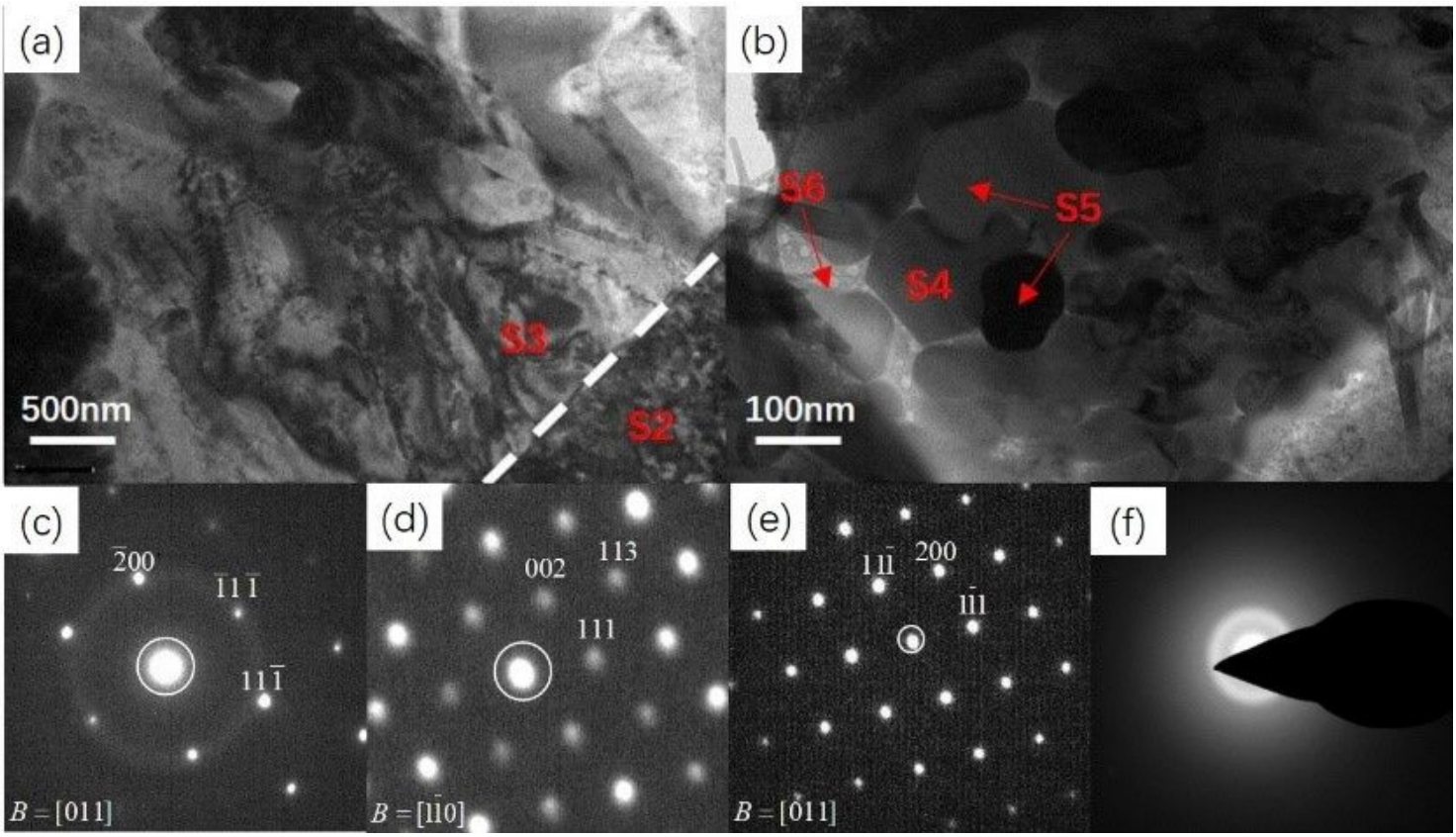

Figure 4

the boundary areas of the reaction zone and unreactive zone are analyzed by TEM, and the results are shown in Fig. 4. Fig. 4 (a) is a transmission electron microscope bright field image of the reaction boundary areas close to Sm2Zr2O7. As shown in Fig. 4 (a), there is an obvious boundary between two different micromorphologies. As shown in the dotted line in the figure. The energy spectrum of the S2 and S3 areas on both sides of the dotted line was analyzed. The results are shown in Table 1. No element of CMAS is found in area S2. Ca and Si elements of CMAS are found in area S3. S3 is SAED analyzed, and the results are shown in Fig. 4 (c). The space group is Fm-3m. However, the lattice constant and the included angle are different from the standard value. This suggests that Ca and Si enter the lattice of Sm2Zr2O7 and cause lattice distortion. Therefore, S2 is Sm2Zr2O7, and S3 is an erosion product. Fig. 4 (b) is a transmission electron microscope bright field image of the reaction boundary areas close to CMAS. As shown in Fig. 4 (b), there are some small grains with different sizes, which include some spherical crystal grains (S4) and some rod crystal grains (S5). The energy spectra of areas S4 and S5 are analyzed, and the results are shown in Table 1. S4 and S5 are SAED analyzed, and the results are shown in Fig. 4 (d) and Fig. 4 (e). The space group of S4 is P63/m, and the space group of S5 is Fm-3m. Combining the XRD results and elemental proportions of S4 and S5, it can be determined that the spherical crystal grain (S4) is Ca2Sm8(SiO4)6O2 and the rod crystal grain (S5) is a c-ZrO2 solution. The light color area of S6 is SAEDP analyzed, and the results are shown in Fig. 4 (f). The electron diffraction pattern of S6 is diffuse scattering, which infers that S6 is amorphous.

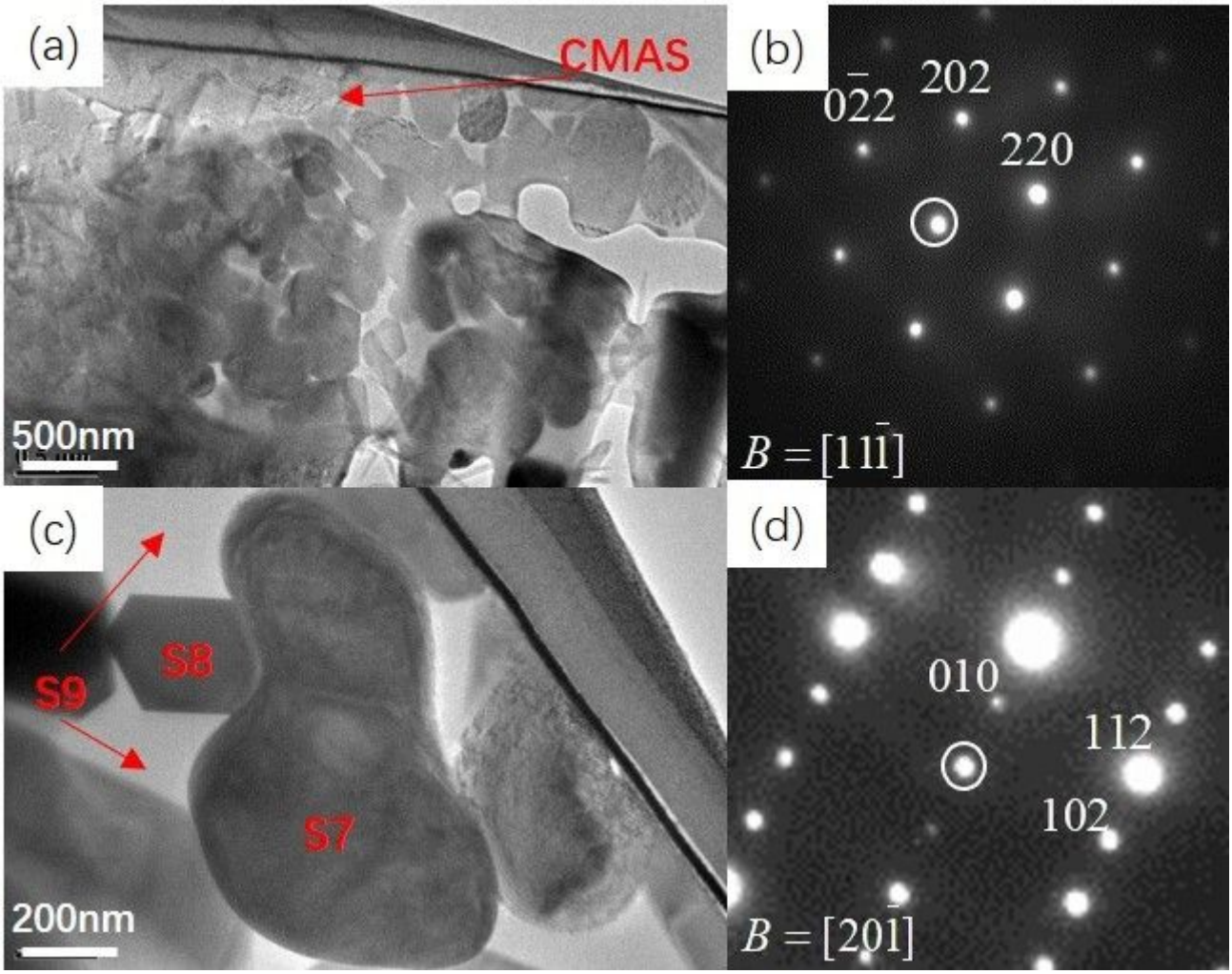

Figure 5

the loose areas after reaction are analyzed by TEM, and the results are shown in Fig. 5. Fig. 5(a) is a TEM bright field image of the loose area after the reaction. As shown in Fig. 5(a), unlike the reaction boundary areas, the grains in this area are relatively loose. There is a large amount of residual CMAS. The closer to the CMAS direction, the larger the grain size. Fig. 5(c) is a TEM high-power bright field image of the loose area after the reaction.

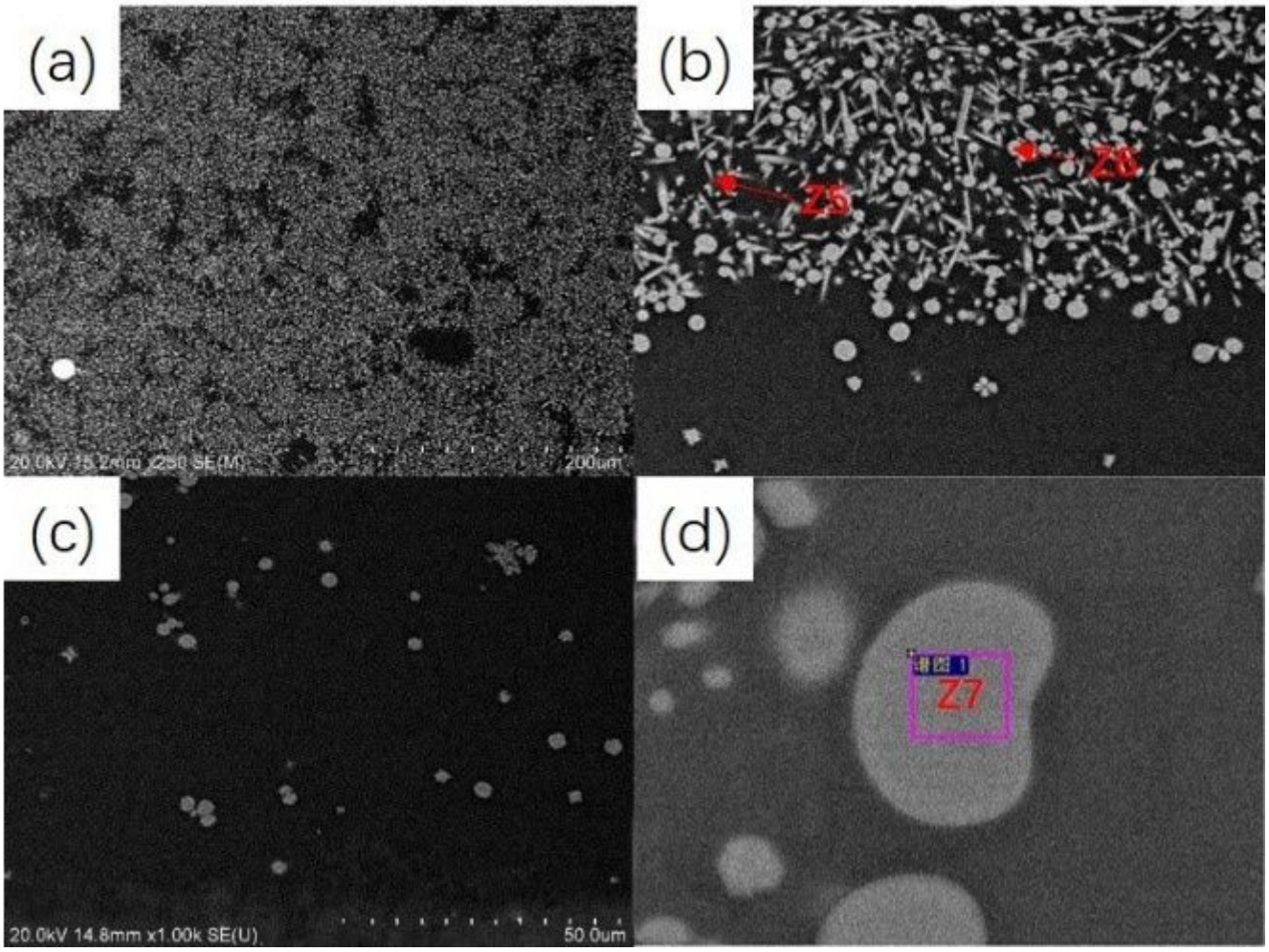

Figure 6

The image of Sm2Zr2O7 powders eroded for 4 h at 1350℃ is shown in Fig. 6(a). As shown in Fig. 6(a), all Sm2Zr2O7 powders are eroded by CMAS. There are no partly eroded powders with core-shell structures. Fig. 6(b) shows only rod crystal grains (Z5) and spherical crystal grains (Z6). The elements of Z5 and Z6 are shown in Table 2. According to the reaction results for 1 h, rod crystal grains (Z5) are c-ZrO2 solution, and spherical crystal grains (Z6) are Sm-apatite.

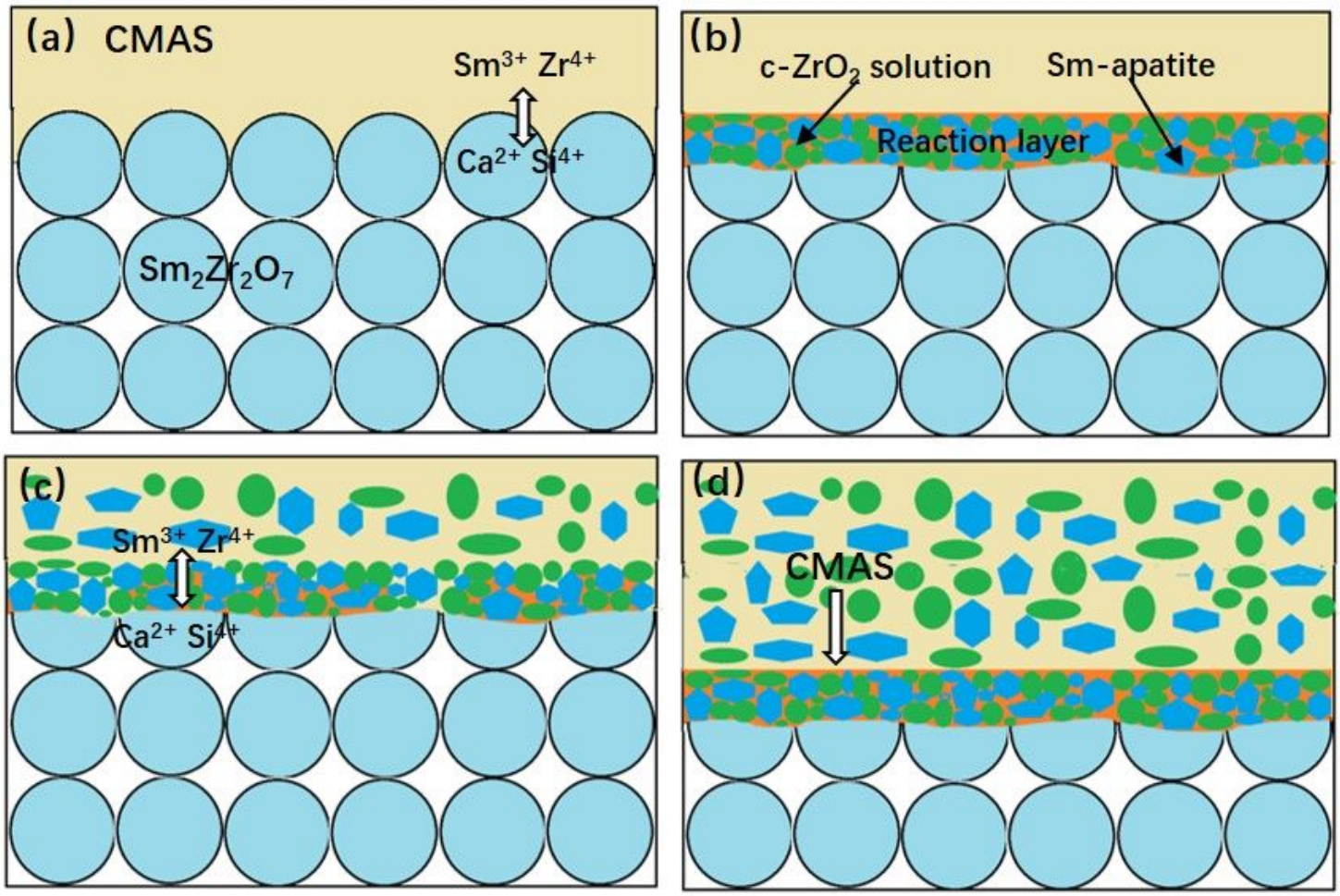

Figure 7

According to the above process, the erosion model of excessive CMAS to Sm2Zr2O7 material is established and shown in Fig. 7.